SLAC-PUB 587
April 1969
(EXPI)

STATISTICS OF TRANSMISSION SECONDARY EMISSION FROM THIN FILMS OF ALKALI-HALIDES*

J. Llacer and E. L. Garwin
Stanford Linear Accelerator Center
Stanford University, Stanford, California 94305

ABSTRACT

The statistical distribution of the number of emitted secondary electrons per primary incident on transmission alkali-halide dynodes has been studied. For high primary energies (1 MeV), a model based on the theory of dielectric energy loss and the secondary electron-phonon interaction is proposed to account for statistical distributions. Measurements of distributions from 500 Å-thick films of CsI, KCl, and LiF have been carried out both at high energies, and for primary energies near 9 keV corresponding to the maximum of secondary yield. It is shown that with some simplifying approximations, the model proposed can be used to calculate the distributions observed with high energy primaries. Qualitatively, it is also possible to use the ideas proposed to understand the experimental results at low energy. Although in the literature the statement is often made that secondary emission distributions can be expected to be Poissonian, it is shown in this paper that there is very little firm basis for such a statement, and it is only through a knowledge of the detailed phenomena controlling secondary emission that a particular distribution can be predicted.

(Submitted to Journal of Applied Physics.)

*Work supported by the U. S. Atomic Energy Commission.

I. INTRODUCTION

The study of the statistical distribution of the number of secondary electrons emitted when a primary electron is incident on a target material has been the object of a substantial amount of research in the last few years. There have been two general experimental approaches to the problem: (1) the observation of the output pulse distribution from a photomultiplier tube when the cathode was illuminated with a feeble light source, in which case the combined response of the first few dynodes to a single photoelectron from the cathode is studied, and (2) the direct counting of the number of electrons emitted from a target per incident primary electron, which is accomplished by a fixed acceleration of the secondaries and measurement of the total energy in the accelerated packet.

Lombard and Martin[1] made the initial calculation of the pulse height distribution at the output of a multiplier assuming a Poisson distribution at each stage, and found that such an assumption did not give correct results in comparison with experiments carried out by the first method. Delaney and Walton[2] found that, with commercially available photomultipliers, careful directing of the light beam so as not to strike the first dynode resulted in an output pulse distribution which closely resembled the theoretical results of Lombard and Martin (Poisson assumption). More recently, Prescott[3] has shown that if one assumes that a secondary emitter is non-uniform so that different parts of it each obey Poisson statistics but with different means, the output pulse distribution of a multiplier structure will follow a Polya statistical distribution. The Polya distribution has as its two limiting cases exponential and Poisson distributions, and can be tailored to fit a wide range of experimental results. Prescott's conclusion is, however, that there is not sufficient evidence to determine whether dynode inhomogeneities alone are sufficient to account for the deviations from Poisson statistics at each dynode, or whether the process of secondary emission is in itself non-Poissonian.

Measurements of this same type have also been carried out on a transmission secondary electron image intensifier with KCl dynodes by Reynolds, Hutchinson and Botos[4] with results which deviated very strongly from a Poisson distribution. More recently, Dietz, Hanrahan and Hance[5] made measurements on a low density (porous) KCl transmission dynode (with yields in the range of 30 to 40) followed by a standard multiplier structure. The statistical distribution of output pulses was found to be only partially describable by the pure exponential limit of Polya statistics, with deviations at the higher pulse amplitudes.

Measurements of the second kind, which can give directly the statistical distribution of emitted electrons (except for corrections due to less than perfect electron detection), have been carried by Haüssler[6] in reflection from CuBe and KCl dynodes using a scintillator-photomultiplier combination as the electron detector. Data were collected in a multichannel analyzer. For both materials, the distributions obtained were broader than a corresponding Poisson distribution with the same mean. Finally, Delaney and Walton[7] have published measurements in transmission from Al and KCl thin films using alpha particles as primaries and a Li-drifted Silicon junction as an electron detector. For Al, again a distribution broader than Poissonian was obtained. Results for KCl were considered doubtful because of suspected deterioration of the emitter film.

Examination of the work published to date indicates that a great deal of emphasis has been placed on the convenient and desirable Poisson distribution. However, there has been no indication that the physical processes involved in secondary emission need result in a Poisson distribution. The work to be reported in this paper attempts to study theoretically the physical processes of energy loss suffered by a primary electron and the escape of the internal secondaries for the case of 1 MeV primary electrons incident on alkali-halide transmission dynodes. The absence of multiple scattering makes this special case easy to analyze, and the particular results are of

interest for the evaluation of transmission dynodes as relativistic particle detectors. Next, we describe experiments carried out to measure the actual statistical distribution for the case treated theoretically, as well as for lower primary energies (near the maximum of secondary yield of the films). Finally, the agreement between the theoretical and experimental results is verified for 1 MeV primaries, and it is shown that the experimental results at lower primary energies and the measurements in reflection can be explained qualitatively from the same theory.

II. THEORETICAL MODEL

A. Primary Electron Energy Loss.

The dielectric theory of energy loss suffered by a primary electron traversing a thin layer of material with complex dielectric constant $\epsilon = \epsilon_1 + i\epsilon_2$ developed by Nozières and Pines[8] provides a starting point for this calculation. It has been shown by those authors that the probability per unit time that a fast primary electron will lose an amount of energy $E = \hbar\omega$ and transfer a momentum $\hbar\underset{\sim}{k}$ per unit volume of target material is given by

$$W(\underset{\sim}{k},\omega) = \frac{-8\pi e^2}{k^2} \operatorname{Im}\{1/\epsilon(\underset{\sim}{k},\omega)\} \tag{1}$$

In order to find the total rate of scattering into a particular element of solid angle $d\Omega$, with an energy loss E, it is necessary to integrate over all possible final states $\underset{\sim}{k}$, bearing in mind that energy and momentum have to be conserved.

With the vector relationships in momentum space of Fig. 1, with $\underset{\sim}{p}$ representing the incident primary electron and $\underset{\sim}{p}'$ the scattered primary, the integral over all finial $\underset{\sim}{k}$ can be transformed into an integral over all final $\underset{\sim}{p}'$

$$W(E)\,dE = -\iint_{\Omega\,p'} d\Omega dp' \frac{p'^2 e^2}{\hbar^2\pi^2(p^2 + p'^2 - 2pp'\cos\theta)} \operatorname{Im}\left\{1/\epsilon(E)\right\}\delta\left\{\frac{p'^2}{2m} - \left(\frac{p^2}{2m} - E\right)\right\} dE \tag{2}$$

where it has been assumed that the dielectric constant ϵ is independent of $\underset{\sim}{k}$ for the very small values of momentum transfer (small scattering angles θ) at which this theory is most useful.[9]

Carrying out the integration over $\underset{\sim}{p}'$ and defining the differential inverse mean free path $d(1/\lambda)$ as $W/v = Wm/p$,

$$d(1/\lambda) = -\frac{1}{2\pi^2 a_0}\frac{1}{E_p}\frac{1}{(\theta^2+\theta_E^2)}\,\mathrm{Im}\left\{1/\epsilon(E)\right\}d\Omega dE \qquad (3)$$

where a_0 is the Bohr radius, E_p is the energy of the primary electron, and $\theta_E = E/2E_p$. This form has been reported by Raether[10] and used by Creuzburg[11] in the successful comparison between electron energy losses and optical measurements of $\mathrm{Im}\left\{1/\epsilon(E)\right\}$ in thin films of alkali-halides, Cu, Ag, and Au, for $E_p = 50$ keV, $\theta = 0$. Equation (3) includes all second order terms in θ and in θ_E.

For 50 keV electrons, Creuzburg and Raether[12] found that the mean free path between collisions in KCl and KBr was about $5 - 10 \times 10^3$ Å so that the probability of having more than one collision in a film of a few hundred Å thickness should be quite negligible in alkali-halides, especially at the higher $E_p = 1$ MeV at which the present work has been carried out.

With this assumption, and neglecting relativistic effects, the probability that a primary electron will suffer a collision with an energy loss between E and E + dE in a film of thickness D will be given by

$$P(E)dE = -\int_0^{\theta_m}\frac{D}{\pi a_0 E_p}\frac{\theta d\theta}{(\theta^2+\theta_E^2)}\,\mathrm{Im}\left\{1/\epsilon(E)\right\}dE = -\frac{D}{2\pi a_0 E_p}\ln\left\{\left(\frac{\theta_m}{\theta_E}\right)^2+1\right\}\mathrm{Im}\left\{1/\epsilon(E)\right\}dE \qquad (4)$$

where θ_m is the maximum angle subtended by the detector of scattered primary electrons.

Equation (4) has two quite distinct limits depending on the relative magnitudes of θ_m and θ_E. If $(\theta_m/\theta_E) \gg 1$, then $P(E) \propto \ln(C/E)\cdot \mathrm{Im}\left\{1/\epsilon(E)\right\}$, with $C \gg E$, while in the

opposite case $P(E) \propto 1/E^2 \cdot \mathrm{Im}\{1/\epsilon(E)\}$. For the case of interest with $E_p = 10^6$ eV, and energy losses ranging between a few eV and up to 10^3 eV, for example, the first case would seem to apply when the angle subtended by the detector is larger than 10^{-3} radians. The second case would apply for $\theta_m \lesssim 10^{-6}$ radians. The question which arises is with regard to the assumption that the dielectric constant is independent of $\underset{\sim}{k}$ in a given experiment. A deflection of 10^{-3} radians on a 1 MeV electron corresponds to a magnitude of wave-number $|k|$ (Fig. 1) of $.44 \times 10^{10} m^{-1}$, which is of the order of the dimensions of the Brillouin zone. Although no calculations seem to exist on the $\underset{\sim}{k}$ dependence of the dielectric constant of insulators, it cannot be assumed a priori that $\epsilon(\underset{\sim}{k}, E)$ will remain a constant near $\epsilon(\underset{\sim}{0}, E)$ over such a large range. If the assumption were made that ϵ is only independent of $\underset{\sim}{k}$ for about 1/1000th of the dimensions of the Brillouin zone and $\mathrm{Im}\{1/\epsilon(E)\}$ tends to zero for larger $|k|$, then one could expect $P(E) \propto 1/E^2 \cdot \mathrm{Im}\{1/\epsilon(E)\}$ to be found experimentally even if a detector with θ_m larger than 10^{-6} radians were to be used in the experiments. This hypothesis will be tested in part in the experiments described in Part III, below.

Making use of the ideas developed above, a simple model can be devised for obtaining the probability distribution of internally generated secondary electrons, $P_i(n)$, per incident primary electron. For a material with an energy gap E_g, the probability that a primary electron will generate one internal secondary will be given by

$$P_i(1) = \int_{E_g}^{2E_g} P(E)\, dE \quad . \qquad (5)$$

When the energy loss is above $2E_g$, the "hot" secondary generated can interact further with valence or inner shell electrons forming a cascade of electrons with final energies between E_g and $2E_g$ above the valence band energy. This cascade is expected to occur very near the location where the main interaction with the primary electron occurred. This can be justified by an order of magnitude calculation from

the formula for energy loss per unit length developed by Dekker and van der Ziel[13] in the approximation for strongly bound electrons

$$-\left(\frac{dE_p}{dx}\right) = \frac{2\pi e^4}{E_p} N_a \sum_{\underset{\sim}{k'}} \sum_{\underset{\sim}{k}} f_{\underset{\sim}{kk'}} \ln\left(\frac{2E_p}{E_{\underset{\sim}{kk'}}}\right) \tag{6}$$

In this formula E_p can be taken to be the energy of the "hot" secondary electron. The summation over all possible final states $\underset{\sim}{k}'$ and initial states $\underset{\sim}{k}$ of the oscillator strength $f_{\underset{\sim}{kk'}}$ is equal to the number of electrons per atom that can take part in the transitions. The factor $\ln (2E_p/E_{kk'})$ can be taken as a constant at its smallest value, when $E_p = E_{\underset{\sim}{kk'}}$. With $N_a = .3 \times 10^{23}$ molecules per cc. of KCl, and at low E_p only the 6 outer electrons of the Cl^- ion available for interactions, Eq. (6) gives a minimum energy loss of $180/E_p(eV\text{-}\mathring{A}^{-1})$.

The number of electrons developed in the cascade as a function of the energy lost by the primary electron will be simply assumed on the average, equal to the integer next largest to $(E-E_g)/E_g$, i.e., in general

$$P_i(n) = \int_{nE_g}^{(n+1)E_g} P(E)\, dE \tag{7}$$

and

$$P_i(0) = 1 - \int_{E_g}^{\infty} P(E)\, dE \tag{8}$$

The energy distribution of the internal secondaries generated as single electrons is given directly by the form of P(E), but the situation is complicated for electrons generated in groups of two or more. It will be assumed, however, that the end product of the electron cascades has an energy distribution similar to the case for single secondaries.

B. The Escape of Internally Generated Secondary Electrons.

The mechanism of escape of internal secondary electrons in alkali-halide films has been studied in detail by Llacer and Garwin.[14,15] It has been found that the interaction between the internally excited secondary electrons and the longitudinal optical phonons is the dominant factor determining the probability that a particular excited electron will be able to reach the surface of the emitter. It was also found that the role of the surface barrier in the alkali-halides is very small, especially in the case of materials with higher yield. For internal secondary electrons generated isotropically with an initial energy $\mathscr{E}_0$ above the conduction band edge at a certain distance x from the surface, it was found that the escape probability was approximately exponential in character, particularly for films above 250 Å in thickness, so that a characteristic escape length $L_s(\mathscr{E}_0)$ could be defined. Likewise, a constant $P_0(\mathscr{E}_0)$ corresponding to the probability of escape of electrons generated isotropically at the film exit surface was given. Under those conditions the probability that a given internal secondary electron will be able to escape to the vacuum can be given by

$$P_s(\mathscr{E}_0, x) = P_0(\mathscr{E}_0) \exp\left\{-x/L_s(\mathscr{E}_0)\right\} \qquad (9)$$

A graph of the best values for P_0 and L_s for CsI, KCl and LiF, covering materials from the highest to lowest yield, is given in Figs. 2a and 2b. The approximately linear behavior of P_0 and the approximately logarithmic behavior of L_s are clearly seen. With a film thickness D much less than the mean free path between collisions for the primary electron, the probability that an interaction will occur is uniform throughout the film thickness. If a number n of internal secondary electrons are the the end product of a given interaction, the escape of each individual electron will be independent of the escape of the others. If the energy distribution of the internal secondaries is given by a function $G(\mathscr{E}_0)$, it is then possible to define the mean probability α that a single internal secondary electron will escape from the emitter for a given

material as

$$\alpha = \frac{\int_0^{E_g}\int_0^{D} P_s(\mathcal{E}_0, x)G(\mathcal{E}_0)dx\, d\mathcal{E}_0}{D\int_0^{E_g} G(\mathcal{E}_0)d\mathcal{E}_0} \tag{10}$$

From the binomial distribution, the probability that m external secondaries will leave the film when n internal secondaries are generated is

$$P_n(m) = \frac{n!}{m!\ (n-m)!}\alpha^m(1-\alpha)^{n-m} \tag{11}$$

Further, if there exists an internal distribution of generated secondaries $P_i(n)$, the external distribution of escaping secondaries $P_{ext}(m)$ is obtainable from Eq. (11) as

$$P_{ext}(m) = P_i(m)\alpha^m + \sum_{n=m+1}^{n_{max}} P_i(n)\frac{n!}{m!\ (n-m)!}\alpha^m(1-\alpha)^{n-m} \tag{12}$$

where n_{max} is some practical cutoff for the summation. The evaluation of this expression is the main object of the present work, and it will be carried out after the experiments are discussed next.

III. THE MEASUREMENT OF STATISTICAL DISTRIBUTIONS

A. Method and Equipment.

The method used for the measurement of statistical distributions of secondary emission is basically of the same type used by Delaney and Walton.[7] The system is shown schematically in Fig. 3. For measurements with low energy primary electrons, (5 to 10 keV) a low temperature hairpin filament is used. A bias electrode and anode combination focus the beam of electrons onto the transmission dynode. Beam cross sections used are near 1 cm^2. The dynode support consists of a ring with a 2.5 cm dia. aperture on which a 1000 -Å film of Al_2O_3 is attached.[16] Next, a 500 Å layer of Al is evaporated forming the complete substrate. The alkali-halide films are then

evaporated onto the substrate at pressures near 10^{-8} torr and transferred to the tube in an atmosphere of dry N_2 (less than 1.5% relative humidity). The dynode is held at + 90 volts with respect to the anode in order to avoid secondary emission from the primary entrance side. A grid with 94% transmission, 2 lines/mm is placed at the exit side of the dynode and connected to it by a floating 0 to ± 90 volts battery power supply. The accelerating structure, consisting of 3 elements focuses emitted secondaries into a 8 mm dia. aperture at the end of the tube. The trajectory of these electrons, which have been accelerated to 23.5 keV, is then bent by a permanent magnet so that they strike a surface barrier Li-drifted Si radiation detector D2. Electrons scattered back from the detector are returned to it by the action of the magnetic field. By turning the magnet in the opposite direction, the beam can be made to strike a ZnS screen for optical observation of the beam and for transmitted current measurements. For measurements with high energy primary electrons, a radioactive Sr-Y^{90} source is placed at a window in a line of sight with the center of the dynode and with another Li-drifted Si radiation detector D1, which subtends an angle of .025 radians from the center of the dynode. The windows separating the source and detector (at atmospheric pressure) from the vacuum system are made of thin Al foil, as described by Edgecumbe.[17] The Sr-Y^{90} source emits electrons up to nearly 2 MeV. The system, which is vented only to dry N_2, is evacuated by chilled molecular sieve and ion pumps, with an unbaked ultimate pressure nearly 10^{-8} torr. Detector D2, which operates in vacuum, is cooled to liquid nitrogen temperature through a cold finger.

The electronic system is shown schematically in Fig. 4. The signal from detector D2, consisting of a pulse with an area proportional to the number of electrons detected, is first amplified by a FET charge sensitive amplifier, and then by a second amplifier with an integrating and differentiating time constant of 2 microseconds. The output goes to the 400 channel pulse-height analyzer. In measurements at low primary

energies this is the only electronics used. For measurements at high energy, the output of detector D1, after suitable amplification, feeds a single channel analyzer. With its lower and upper level controls properly set, one output pulse is obtained when the energy collected by detector D1 is 1 MeV, ± 150 keV, as determined by pulser measurements. (Thickness of detector intrinsic region = 2 mm.) After suitable delay and shaping, this pulse is used to activate the delayed coincidence circuit of the analyzer and is used to effect selection of the events recorded. Counter C1 records the number of primary electrons admitted for analysis, while C2 counts the number of times that the multichannel analyzer records a count of any height. This allows the determination of the probability P(0), that a high energy primary will generate no external secondaries.

B. Calibration and Data Analysis.

Letting $I_{D\pm}$ be the measured dynode current with the grid at ±90 V with respect to the dynode, and η_t be the transmission coefficient of the dynode for primaries of a particular energy E_p, the primary current in the tube of Fig. 3 is given by

$$I_p = \frac{-I_{D-}}{1-\eta_t} \tag{13}$$

neglecting backscattering from the dynode. With the secondary yield δ defined as the magnitude of secondary current divided by the primary current, it is found that, approximately,

$$\delta = (1-\eta_t)\left[1 - \frac{I_{D+}}{I_{D-}}\right] \tag{14}$$

Measurements of δ in this tube are not expected to be particularly accurate, since η_t is not measurable and is obtained from separate measurements of similar films in other tubes. (Reference 18 describes some of the precautions needed to make yield measurements to accuracies better than ± 10% with high gain dynodes.) Nevertheless,

measurements with bare substrates, and with several alkali-halide dynodes gave results consistent with those reported in Ref. 15.

With the voltages in the accelerating electrodes optimized for maximum transmission onto the ZnS screen, and electron-optical transmission coefficient of $\beta = .82 \pm .02$ was obtained by comparing $(I_{D+} - I_{D-})$ with the current collected at the screen. The effect of this coefficient being less than unity manifests itself as a distortion of the experimentally obtained probability distributions. In fact, for totally independent electrons leaving the dynode, the probability that m electrons will reach the detector if n electrons left the dynode is again given by Eq. (11) with β replacing α, while the probability distribution at the detector end can be obtained from an expression similar to Eq. (12) in terms of the distribution at the dynode exit.

The detector response has to be analyzed carefully, as the peaks obtained in the analyzer start overlapping seriously as the number of electrons emitted increases. Figure 5 shows the Gaussian spectrum of the amplifier noise (with detector connected) recorded at high amplifier gain. It corresponds to 3.9 keV FWHM. Superimposed, a spectrum obtained from single electrons leaving the dynode has been recorded. The difference is due to backscattering, losses in the Au window of the detector, trapping, etc. Since these phenomena are independent of the electronic noise, the combined response will be the convolution of some detector function f(E) with the noise Gaussian. A function of the form $f(E) = \exp\left\{a(E-E_0)\right\}$ for $E < E_0$ and $f(E) = 0$ for $E \geq E_0$ (E_0 is the center of the Gaussian) has been successfully fitted to the detector function so that the combined response can be reproduced by convolution. Once the detector spectrum can be reproduced mathematically for the single electron peak, the spectrum for m electrons is easy to obtain by (m-1) convolutions of the function f(E) with the single electron spectrum, assuming independent treatment by the detector of each individual electron.

In the experiment, the electronic gain of the system is adjusted to 23.25 keV (the accelerating potential) at channel 8 in the pulse-height analyzer, enabling the analyzer to record information for up to 50 secondaries emitted simultaneously. The method of data analysis can be outlined as follows: Let the matrix $\underset{\sim}{A}$ (50×50) contain as elements A_{ij} the area under the normalized mathematical detector spectrum for i electrons included between channels (8j-7) and (8j). Let also $\underset{\sim}{z}$ (50) be a vector with elements z_j corresponding to the probability distribution of electrons entering detector D2. Then the expected spectrum in the analyzer, summed every 8 channels, will form a vector $\underset{\sim}{b}$ obtainable from $\underset{\sim\sim}{A}\underset{\sim}{z} = \underset{\sim}{b}$. The electron optical transmission of the accelerating structure can be put in a convenient form by defining a matrix $\underset{\sim}{D}$ with elements

$$D_{ij} = \frac{j!}{i!\,(j-i)!}\,\beta^{i}(1-\beta)^{j-i} \qquad (15)$$

from Eq. (11).

Defining another vector $\underset{\sim}{x}$ containing the probability distribution of electrons at the exit of the dynode, it is found that vector $\underset{\sim}{z}$ can be obtained from $\underset{\sim\sim}{D}\underset{\sim}{x} = \underset{\sim}{z}$, and the true distribution $\underset{\sim}{x}$ is related to the measured $\underset{\sim}{b}$ by

$$(\underset{\sim\sim}{A}\underset{\sim\sim}{D})\underset{\sim}{x} = \underset{\sim}{b} \qquad (16)$$

The solution for $\underset{\sim}{x}$ has presented some serious difficulties due to bad behavior of the product matrix $(\underset{\sim\sim}{A}\underset{\sim\sim}{D})$ upon inversion. However, a method based upon function fitting by minimization of χ^2 has given quite good results up to m = 25 to 35 electrons depending upon the shape of the spectrum.

The most important sources of error in the analysis are: (1) The expected error in the determination of β. Its effect is only felt substantially at high m. (2) Drift in the baseline of the analyzer (gain has proven to be very stable). A drift of $\pm 1/2$ channel results in substantial fluctuations in the analyzed results at low m. (3) Errors

in the mathematical fitting process. These range between .1% at low m to 5--8% at high m. (4) Statistical errors due to a limited number of counts in a particular peak. These have been made negligible, in general, by counting long enough. For the purpose of illustration, unprocessed data $\underset{\sim}{b}$ and corrected data $\underset{\sim}{x}$ for typical experimental data are shown in Fig. 6. The approximate range of errors expected at different points is also indicated.

C. Results of Measurements.

The probability distribution $P_{ext}(m)$ of emitted electrons has been measured for 500 Å films of CsI, KCl, and LiF for primary energies near 1 MeV, as well as at lower energies, near the point of maximum yield. Figure 7 shows the distributions for the high energy case. Since $P_{ext}(0)$ is measurable by the coincidence method, the secondary yields are calculable directly and are given in the figure. For the low energy measurements, $P_{ext}(0)$ cannot be measured directly, but can be inferred approximately from the measured distribution and the known dc yield of the films.[15] Starting from

$$\delta = \frac{\sum_{m=0}^{\infty} m\, P_{ext}(m)}{\sum_{m=0}^{\infty} P_{ext}(m)} \tag{17}$$

it is found that

$$P_{ext}(0) = \frac{1}{\delta} \sum_{m=1}^{\infty} m\, P_{ext}(m) - \sum_{m=1}^{\infty} P_{ext}(m) \tag{18}$$

The summations between m = 1 and 50 have been obtained experimentally, but terms above m = 50 have not. If the assumption is made that the summations for m > 50 can be neglected to a good approximation, Eq. (18) can be evaluated. The knowledge of $P_{ext}(0)$ allows normalization for the presentation of complete probability distributions at low energy in Fig. 8.

IV. DISCUSSION

A. High Energy Measurements.

In trying to compute the distribution $P_{ext}(m)$ from Eq. (12), the first step is the calculation of $P_i(n)$, the distribution of internal secondaries before the escape mechanism is taken in consideration. For a given material this can be done, for the simple model advocated in this paper, from Eqs. (7) and (8). This calculation, in turn, requires the calculation of P(E) dE, the probability of energy loss by the primary electron, obtainable from Eq. (4) and the values of $\mathrm{Im}\{1/\epsilon(E)\}$ published by Creuzburg[11] for energy losses up to 25 - 35 eV. Since the detector used in the experiments presents a relatively large solid angle to the dynode, initial calculations of P(E) were carried out directly from Eq. (4), with smoothed data from Creuzburg (excitonic losses not expected to contribute to secondary generation). The values of $P_i(n)$ for the first few values of n were then calculable, but decayed much too slowly with n to fit the experimental data of Fig. 7 even after considering the effects due to escape. It was next assumed that, even if the detector is large, only very small deflections of the primary electrons can occur, as conjectured in Part II. In that case, the limit for $\theta_m/\theta_E \ll 1$ can be used in which $P(E) \propto 1/E^2 \cdot \mathrm{Im}\{1/\epsilon(E)\}$. Further, since the smoothed data of Creuzburg change rather slowly in comparison to $1/E^2$, the dependence on the dielectric constant was neglected, leaving

$$P_i(n) = K \int_{nE_g}^{(n+1)E_g} E^{-2}\, dE = \frac{K}{E_g} \frac{1}{n(n+1)} \qquad (19)$$

where K is a normalization constant. The resulting dependence on n appears considerably closer to the form of the experimental results than it did without the assumption of $\theta_m/\theta_E \ll 1$.

The energy distribution of the internal secondaries $G(\mathcal{E}_0)$ has then the form

$$G(\mathcal{E}_0) \propto \frac{1}{(\mathcal{E}_0 + E_g)^2} \qquad (20)$$

which has a good resemblance to the form of $G(\mathcal{E}_0)$ found in Ref. 14. If one uses the energy dependence of Eq. (20) in Eq. (10), along with the data on escape probabilities of Figs. 2a and 2b, the mean probability that a single internal electron will escape can be computed, with the results $\alpha = .37$ for CsI, .25 for KCl and .17 for LiF (500 Å films).

With the normalization constant K of Eq. (19) evaluated by matching the theoretical and experimental points at m = 1, distributions $P_i(n)$ and $P_{ext}(m)$ have been obtained, and are shown in Figs. 7b, 7c, and 7d. $P_{ext}(m)$ has been computed for the values of α computed above as well as for other higher values giving results more in agreement with experiments. The figures show that the simple model proposed in this paper accounts quite well for the probability distribution of emitted electrons at low m, in particular for KCl and LiF. For CsI, examination of Creuzburg's data[10] indicates that the assumption that $\mathrm{Im}\{1/\epsilon(E)\}$ is roughly a constant may not apply well, as that function increases quite markedly with energy loss. This could account for the observed discrepancies which persists even for $\alpha = 0.95$. From the results for KCl and LiF at higher m it is apparent that either the calculated escape probabilities α are too low or $\mathrm{Im}\{1/\epsilon(E)\}$ rises substantially at higher E. The absence of optical data covering continuously the region between E = 30 to 300 eV does not allow a more precise determination of the causes for the observed disagreements.

B. Low Energy Measurements.

The results presented in Fig. 8 are similar to those obtained by Reynolds, Hutchinson and Botos[4] for KCl transmission dynodes. There is a fairly high probability that a primary electron will not generate any secondaries, and $P_{ext}(m)$ decreases with m in a form that could be approximated by the sum of two exponentials. The distributions obtained at low primary energies can only be explained qualitatively because of the complexity of the situation in which the mean free path between primary

electron collisions is smaller than the film thickness, and multiple scattering events may dominate the production of secondaries. In fact, the spatial distribution of energy loss in the film becomes peaked near the exit surface of the film at maximum yield when a large fraction of primaries suffer many scatterings at wide angles.[14] A very simplified picture can be obtained by considering each primary scattering independent of all the others. Then $P_{ext}(m)$ is given by multiple convolutions of the distributions for single scatterings. For the purpose of illustration, the theoretical high energy $P_{ext}(m)$ for CsI, $\alpha = .95$, has been convolved with itself five times and the results are shown in Fig. 9. As the number of scatterings increases, the mean increases, and $P_{ext}(0)$ decreases, both effects in agreement with experimental results.

Regarding the question of whether or not the distribution of emitted electrons should or should not be Poissonian, it is clear from the present work that the process of secondary emission bears little resemblance to a phenomenon like thermionic emission, in which each electron can be considered totally independent of another. In such case, if there is a mean number of electrons emitted per unit time, a Poisson distribution in the number of electrons emitted per unit time can be expected to exist. For the phenomenon of secondary emission each primary electron will produce a certain number of excitations in the emitter, and the resulting cascade of electrons will in part escape from the material. Although each electron in the cascade can be considered independent in its way to the vacuum, the number of internal secondaries originally created depends on a "parent" distribution given by the laws of the electron-electron interaction in solids. At high energies in tranmission it has been shown here that the "parent" distribution can be obtained from the dielectric theory of energy loss, and at lower energies, still in transmission, it may be perhaps obtainable roughly by convolutions of the results for single scattering. The reasons for the observed external distributions are then to be found in a knowledge of the form of the "parent" distribution, and there seems to be very little reason for claiming independence of events in order to justify a Poisson distribution.

The situation is not basically different in reflection secondary emission at low primary energies, as used in photomultiplier tubes. There it has been found that the electron distribution is nearly Poissonian.[3] If the primary electron suffers several scattering events sufficiently close to the surface for the internal secondaries to leave the emitter, and each event results in a distribution with $P_{ext}(0) < P_{ext}(1)$, for example, then multiple convolutions will make the external distribution appear more like a Poissonian, again without having to invoke independence of emission events. This is also shown qualitatively in Fig. 9, starting from the same high energy distribution for CsI, but with $P_{ext}(0)$ arbitrarily lowered to a point below $P_{ext}(1)$.

V. CONCLUSION

In this paper it has been shown that the probability distribution of the number of secondary electrons emitted per high energy primary incident on a thin film of alkali-halide is closely calculable from the dielectric theory of energy loss and from the theory of the electron-phonon interaction controlling the escape of internal secondaries. For the more complex case of lower energies, near the maximum of yield in transmission or reflection, it has been shown qualitatively that the same mechanisms are still basically responsible for the observed distributions. The point has been made that there is no basic reason for expecting those distributions to be Poissonian, except from the fact that any distribution peaked above zero when convolved several times with itself appears Poisson-like in character.

VI. ACKNOWLEDGEMENTS

The authors would like to thank John Edgecumbe, who designed and supervised the construction of the tube for the measurements of statistical distributions, and Charles L. Thurman who made the dynodes and carried out most of the measurements.

REFERENCES AND FOOTNOTES

1. F. J. Lombard and F. Martin, Rev. Sci. Inst. 32, 200 (1961).
2. C. F. G. Delaney and P. W. Walton, Nucl. Inst. and Methods 25, 353 (1964).
3. J. R. Prescott, Nucl. Inst. and Methods 39, 173 (1966).
4. G. T. Reynolds, D. P. Hutchinson and P. Botos, J. Appl. Phys. (Brit.) 17, 489 (1966).
5. L. A. Dietz, L. R. Hanrahan and A. B. Hance, Rev. Sci. Instr. 38, 176 (1967).
6. P. Haüssler, Z. Physik 179, 276 (1964).
7. C. F. G. Delaney and P. W. Walton, IEEE Trans. Nucl. Sci., NS-13, 742 (1966).
8. P. Nozières and D. Pines, Phys. Rev., 113, 1254 (1959).
9. Since optical measurements of the dielectric constant are made with $\underset{\sim}{k} \simeq 0$, predictions of electron energy loss based on optically obtained Im $\{1/\epsilon(E)\}$ can only be compared to electron scattering experiments with a very small detector placed at $\theta = 0$.
10. H. Raether, Springer Tracts in Modern Physics 38, 85 (1965).
11. M. Creuzburg, Z. Physik 196, 433 (1966).
12. M. Creuzburg, and H. Raether, Solid State Comm. 2, 345 (1964).
13. A. J. Dekker and A. van der Ziel, Phys. Rev. 86, 755 (1952).
14. J. Llacer and E. L. Garwin, (to be published in J. Appl. Phys. June 1969).
15. Ibid.
16. A. Roder, "Aluminum Oxide Self-Supporting Films," Report No. SLAC-TN-67-26, Stanford Linear Accelerator Center, Stanford University, Stanford, California (1967).
17. J. Edgecumbe, Rev. Sci. Instr. 37, 1419 (1966).
18. J. Llacer, "Transmission Secondary Emission from Thin Films of Alkali-Halides," Report No. SLAC-86, Stanford Linear Accelerator Center, Stanford University, Stanford, California (1968).

FIGURE CAPTIONS

1. Vector relationships in momentum space.
2. (a) and (b) Parameters relating to the escape of secondary electrons from alkali-halide films.
3. Schematic of the tube for measurements of probability distributions of emitted secondary electrons.
4. Schematic of the electronic system for the measurements of probability distributions of emitted secondary electrons.
5. Response of electronics and semiconductor detector D2 to single accelerated electrons.
6. Effects of correcting analyzer data for detector response and electron-optical transmission. Expected magnitudes of errors are indicated by bars.
7. (a) Corrected experimental data for $P_{ext}(m)$ for 500 Å films of three selected materials at primary energies near 1 MeV.

   (b,c, and d) Comparison of experimental vs. theoretical results for the three cases of Fig. 7a.
8. Corrected experimental $P_{ext}(m)$ for 500 Å films of the three selected materials, at primary energies near the maximum of secondary yield.
9. Illustrating how the process of multiple convolutions due to multiple scattering can give rise to observed statistical distributions at low primary energy.

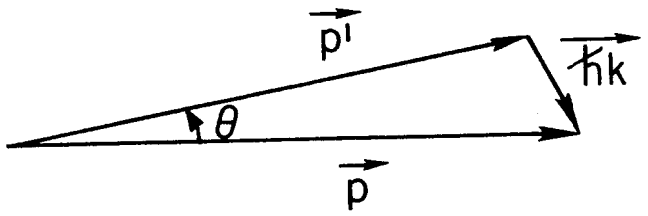

1236A1

Fig. 1

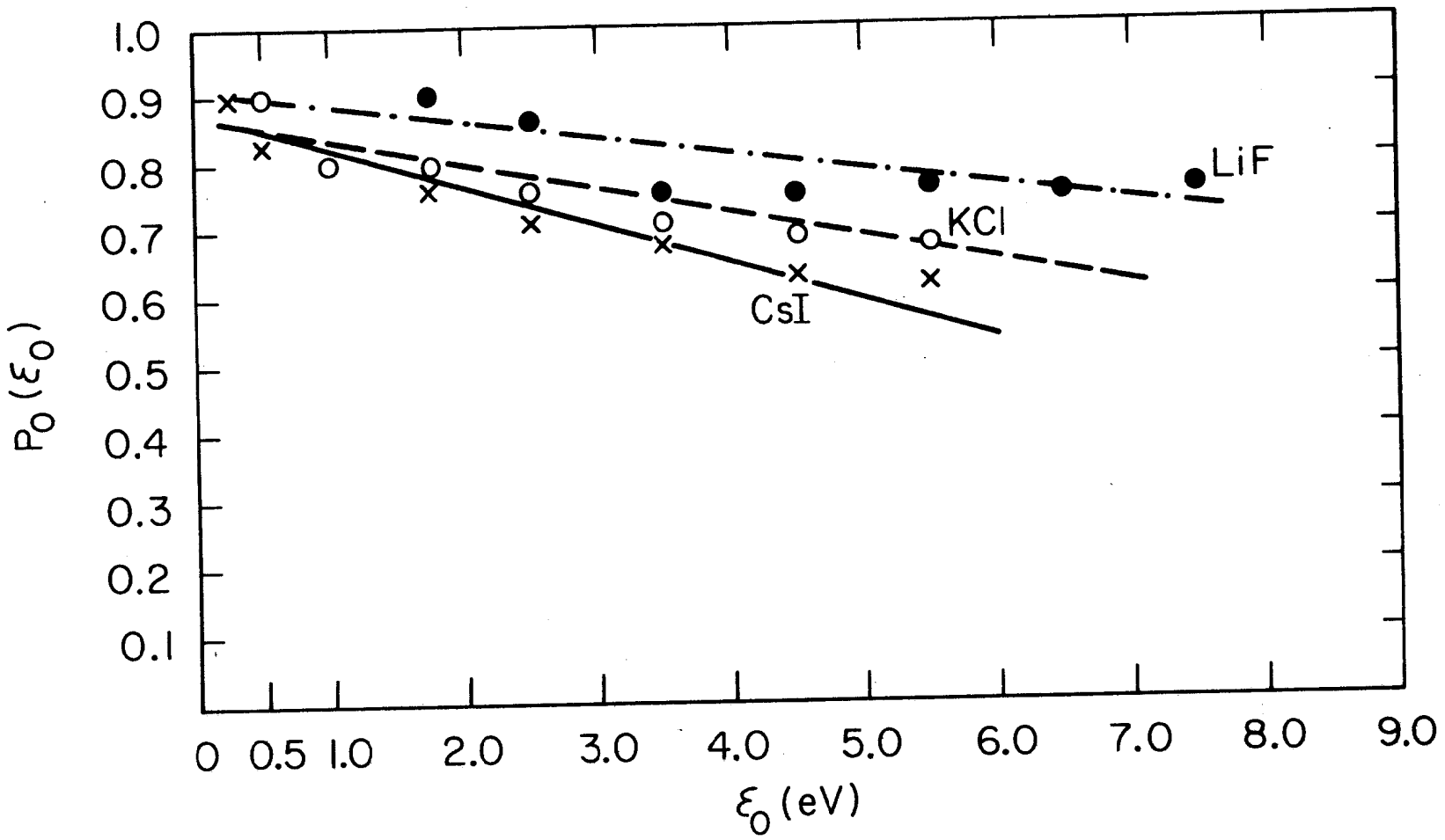

1236A2

Fig. 2a

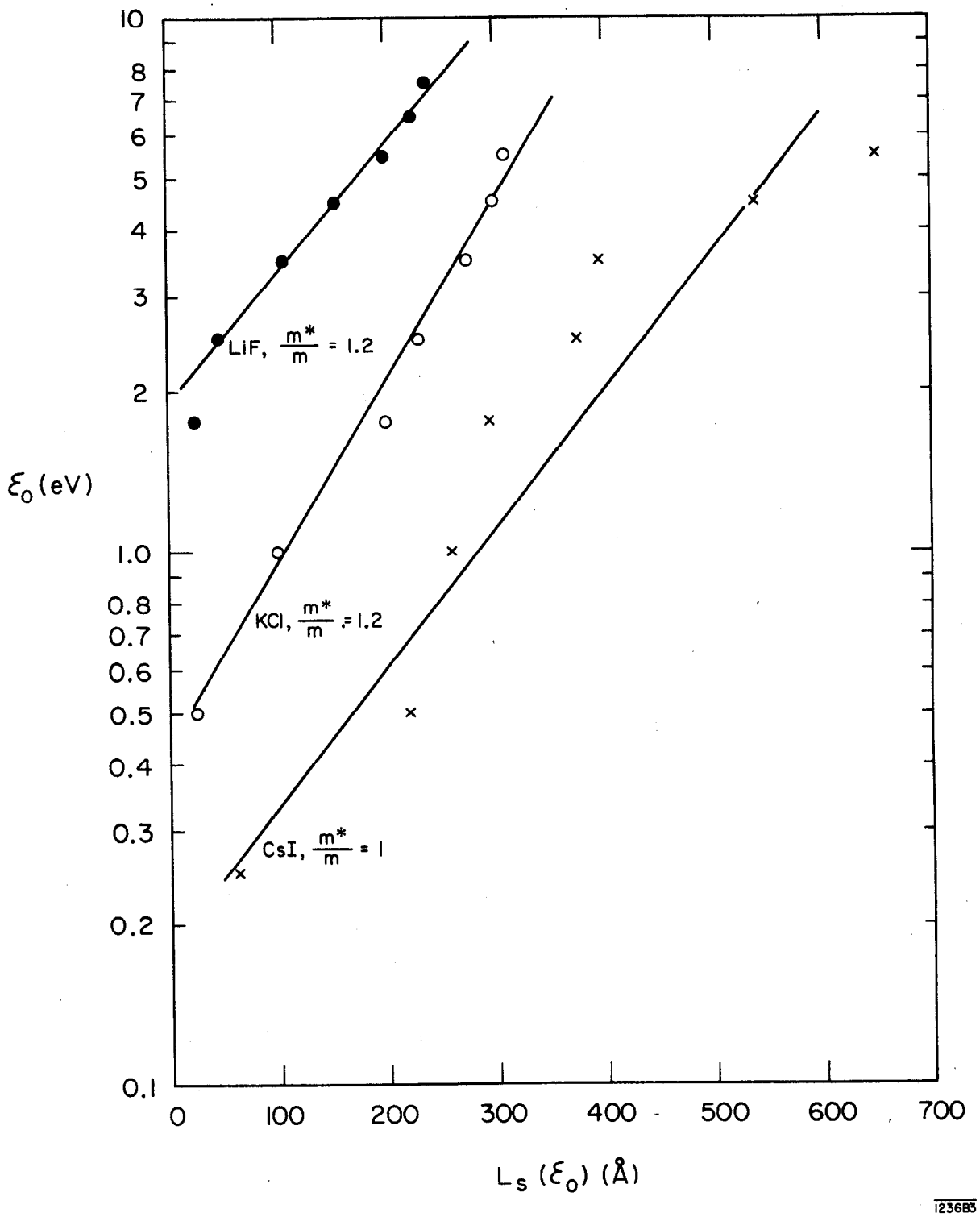
10
8
7
6
5
4
3
2
1.0
0.8
0.7
0.6
0.5
0.4
0.3
0.2
0.1
$\mathcal{E}_0$ (eV)
LiF, $\frac{m^*}{m}$ = 1.2
KCl, $\frac{m^*}{m}$ = 1.2
CsI, $\frac{m^*}{m}$ = 1
0
100
200
300
400
500
600
700
L_s ($\mathcal{E}_0$) (Å)
123683

Fig. 2 b

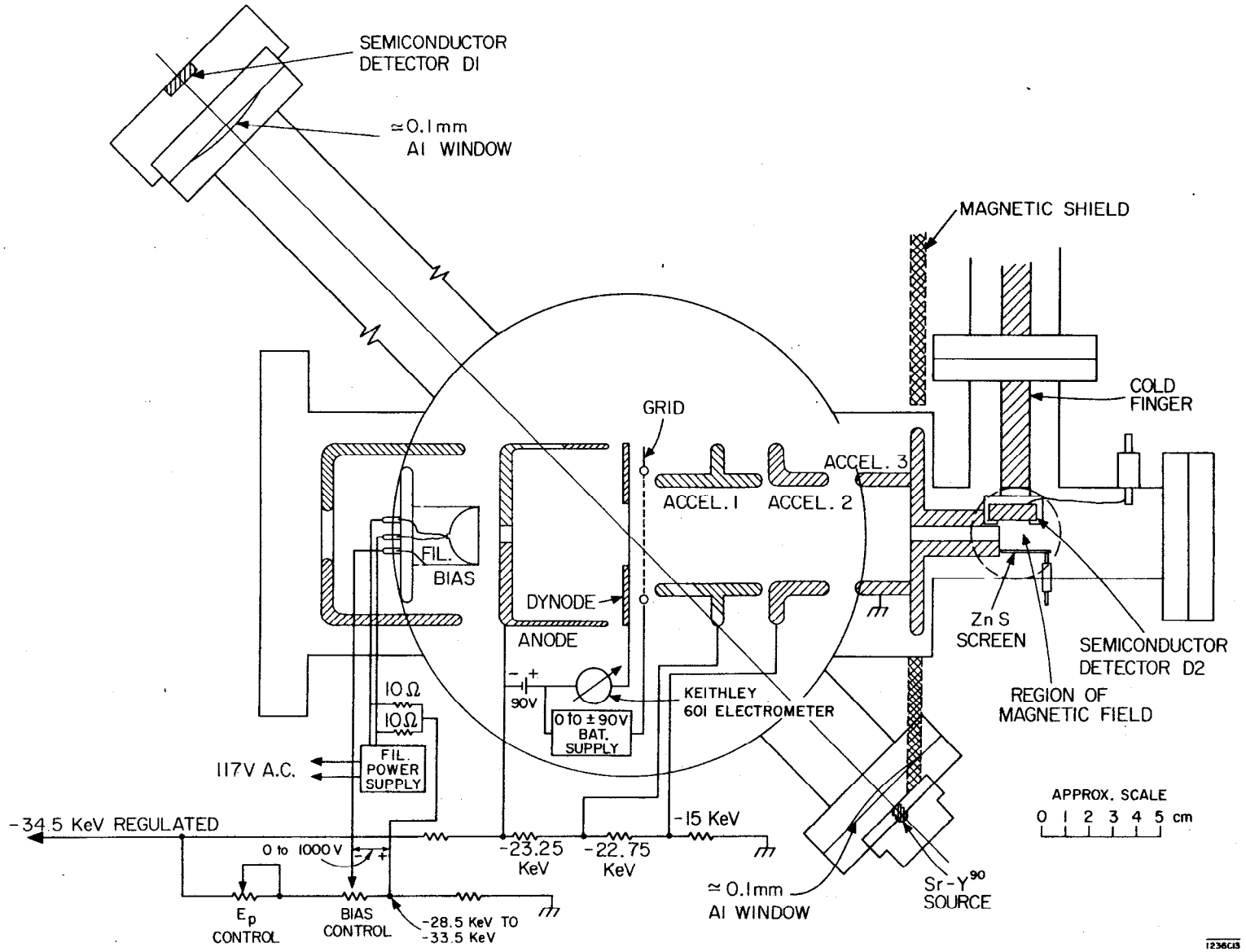
SEMICONDUCTOR
DETECTOR DI
≃0.1mm
Al WINDOW
MAGNETIC SHIELD
COLD
FINGER
GRID
ACCEL. 3
ACCEL. 1
ACCEL. 2
FIL.
BIAS
DYNODE
ANODE
Zn S
SCREEN
SEMICONDUCTOR
DETECTOR D2
REGION OF
MAGNETIC FIELD
10Ω
10Ω
90V
KEITHLEY
601 ELECTROMETER
0 to ±90V
BAT.
SUPPLY
117V A.C.
FIL.
POWER
SUPPLY
APPROX. SCALE
0 1 2 3 4 5 cm
-34.5 KeV REGULATED
0 to 1000V
-23.25
KeV
-22.75
KeV
-15 KeV
≃0.1mm
Al WINDOW
Sr-Y90
SOURCE
Ep
CONTROL
BIAS
CONTROL
-28.5 KeV TO
-33.5 KeV
1236G13

Fig. 3

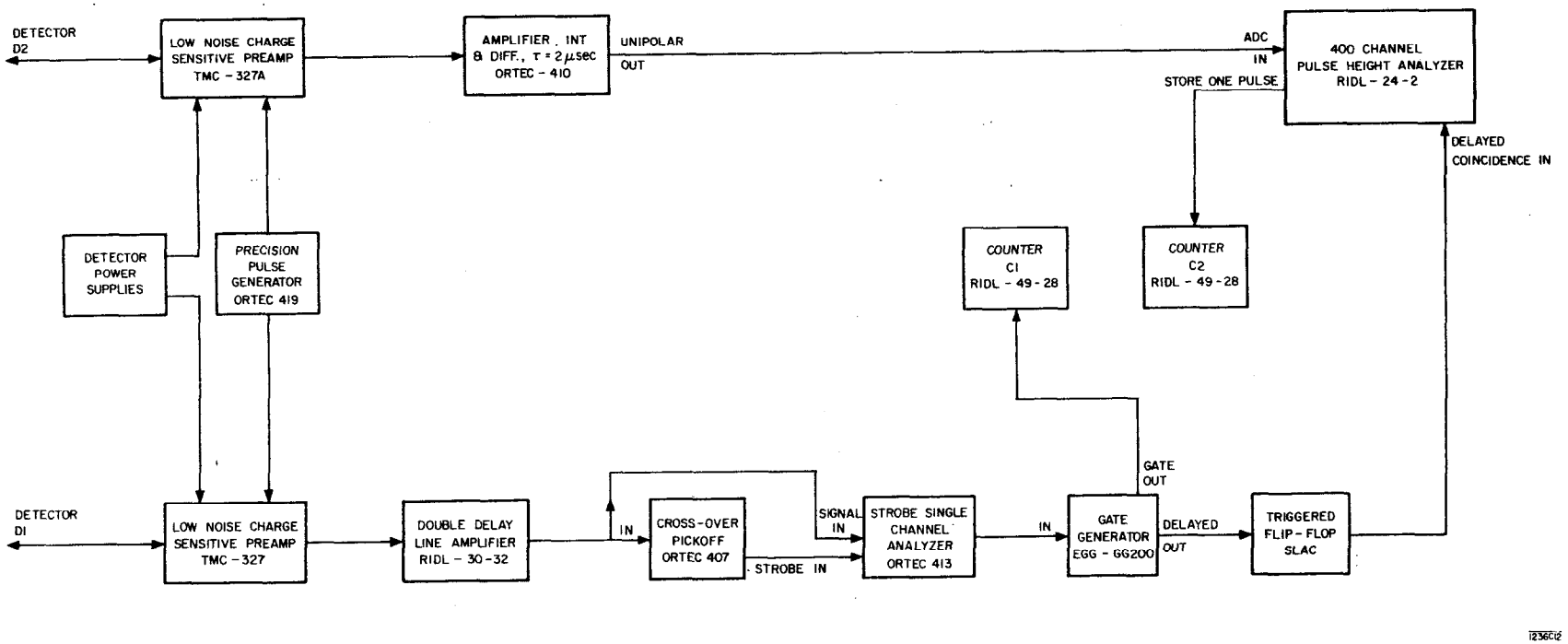
DETECTOR
D2
LOW NOISE CHARGE
SENSITIVE PREAMP
TMC - 327A
AMPLIFIER, INT
& DIFF., τ = 2 μsec
ORTEC - 410
UNIPOLAR
OUT
ADC
IN
STORE ONE PULSE
400 CHANNEL
PULSE HEIGHT ANALYZER
RIDL - 24-2
DELAYED
COINCIDENCE IN
DETECTOR
POWER
SUPPLIES
PRECISION
PULSE
GENERATOR
ORTEC 419
COUNTER
C1
RIDL - 49-28
COUNTER
C2
RIDL - 49-28
GATE
OUT
DETECTOR
D1
LOW NOISE CHARGE
SENSITIVE PREAMP
TMC - 327
DOUBLE DELAY
LINE AMPLIFIER
RIDL - 30-32
IN
CROSS-OVER
PICKOFF
ORTEC 407
SIGNAL
IN
STROBE IN
STROBE SINGLE
CHANNEL
ANALYZER
ORTEC 413
IN
GATE
GENERATOR
EGG - GG200
DELAYED
OUT
TRIGGERED
FLIP-FLOP
SLAC
123601

Fig. 4

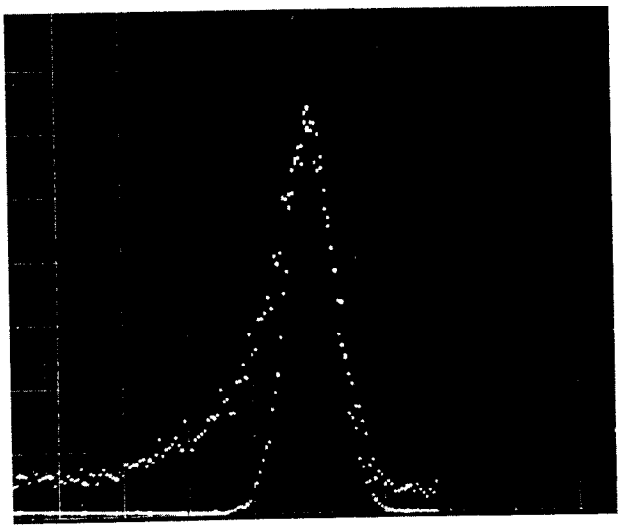

1236A4

Fig. 5

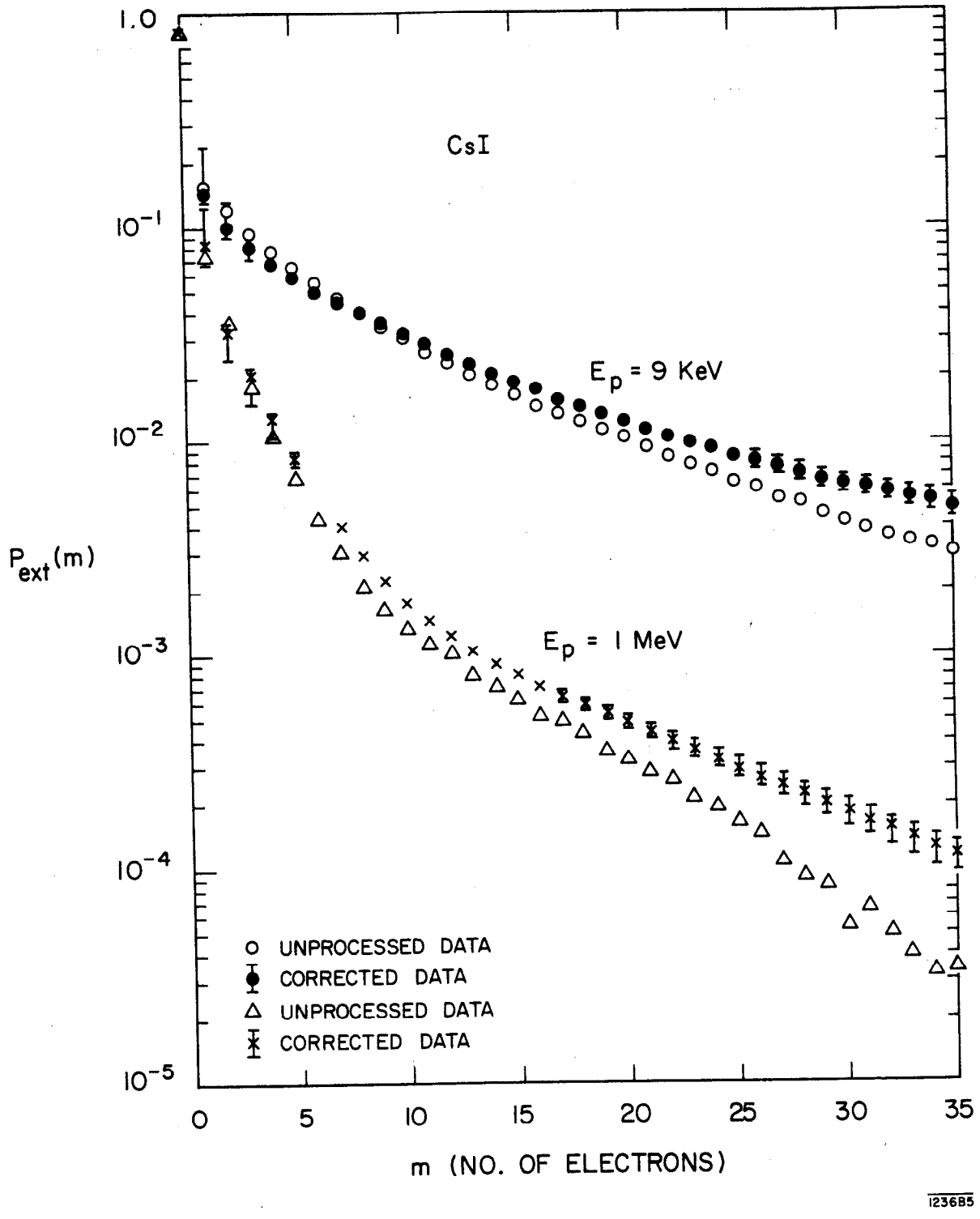
1.0
10^{-1}
10^{-2}
10^{-3}
10^{-4}
10^{-5}
$P_{ext}(m)$
CsI
E_p = 9 KeV
E_p = 1 MeV
o UNPROCESSED DATA
● CORRECTED DATA
△ UNPROCESSED DATA
✕ CORRECTED DATA
0
5
10
15
20
25
30
35
m (NO. OF ELECTRONS)
123685

Fig. 6

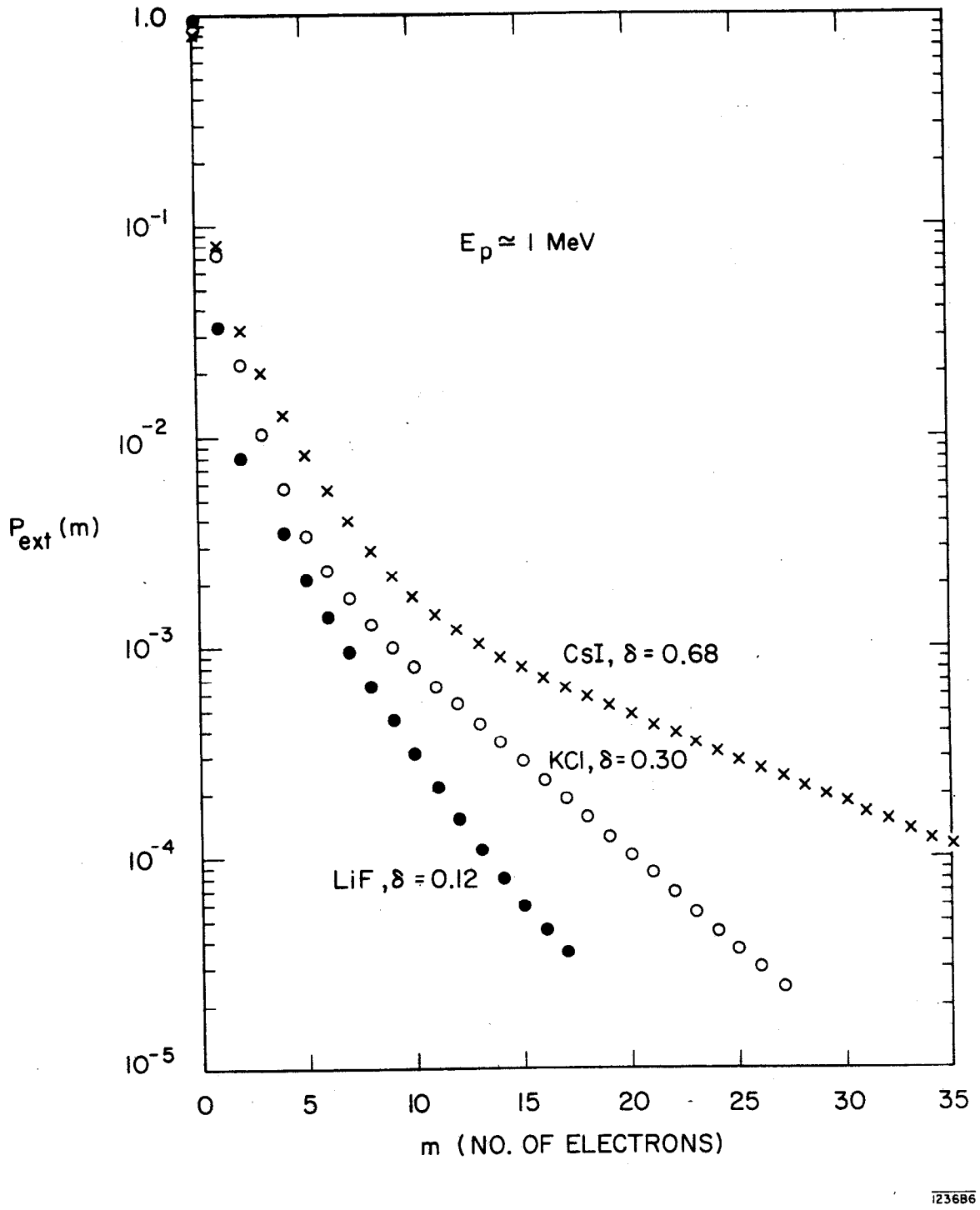
1.0
10^{-1}
10^{-2}
10^{-3}
10^{-4}
10^{-5}
P_{ext} (m)
$E_p \simeq 1$ MeV
CsI, δ = 0.68
KCl, δ = 0.30
LiF, δ = 0.12
0
5
10
15
20
25
30
35
m (NO. OF ELECTRONS)
1236B6

Fig. 7a

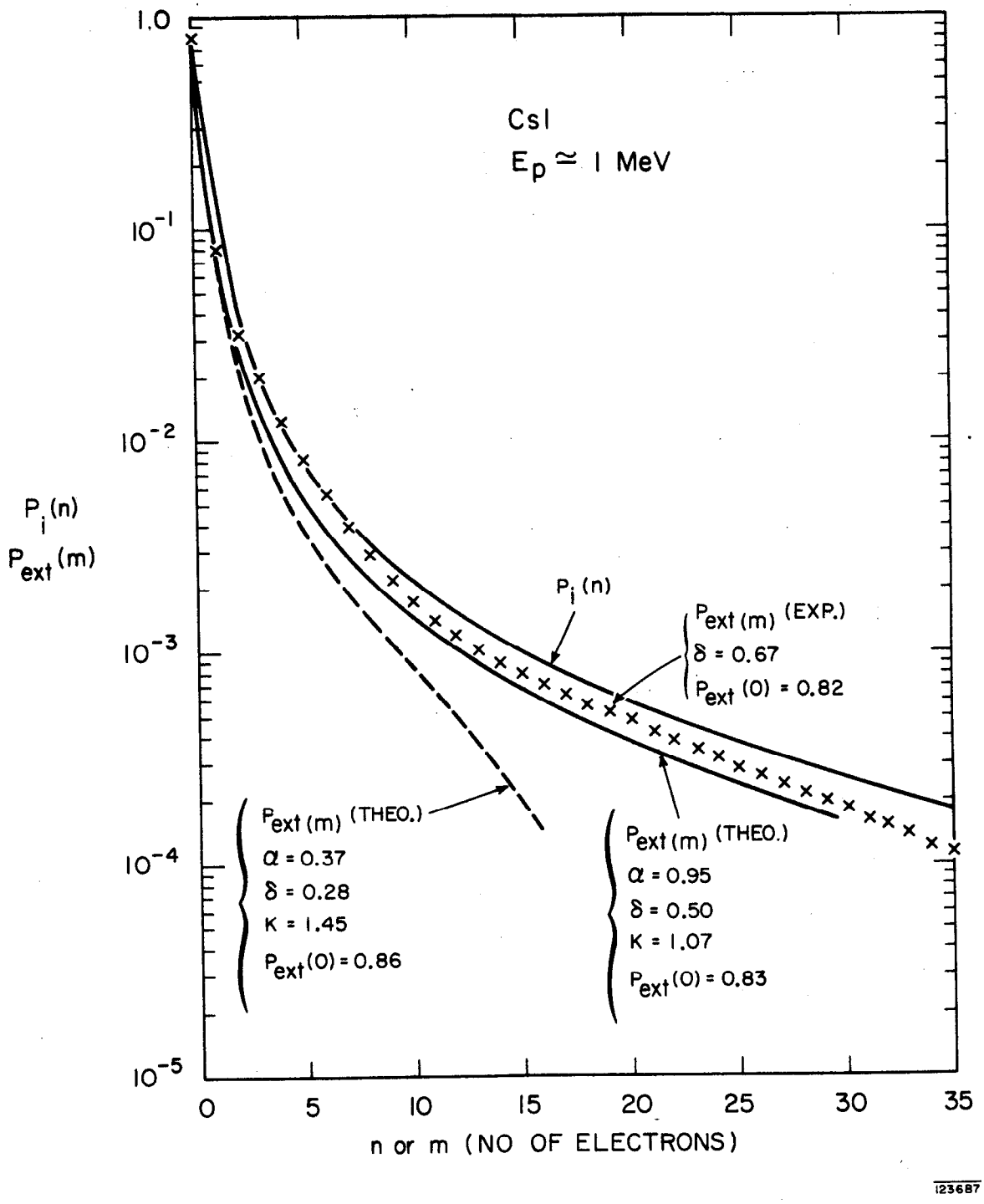
1.0
10^{-1}
10^{-2}
10^{-3}
10^{-4}
10^{-5}
$P_i(n)$
$P_{ext}(m)$
CsI
$E_p \simeq 1$ MeV
$P_i(n)$
$P_{ext}(m)$ (EXP.)
$\delta = 0.67$
$P_{ext}(0) = 0.82$
$P_{ext}(m)$ (THEO.)
$\alpha = 0.37$
$\delta = 0.28$
$K = 1.45$
$P_{ext}(0) = 0.86$
$P_{ext}(m)$ (THEO.)
$\alpha = 0.95$
$\delta = 0.50$
$K = 1.07$
$P_{ext}(0) = 0.83$
0
5
10
15
20
25
30
35
n or m (NO OF ELECTRONS)
123687

Fig. 7b

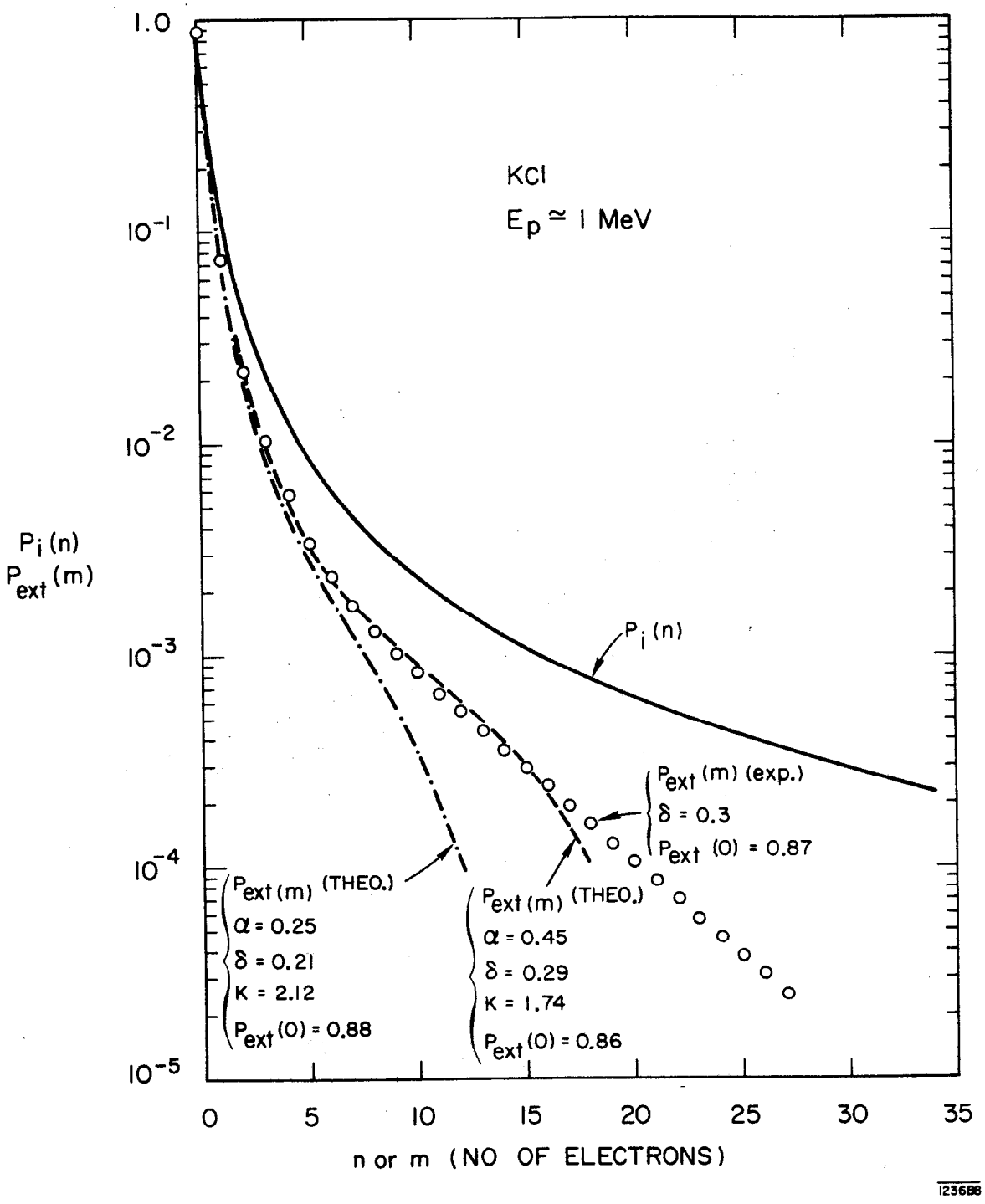
1.0
10^{-1}
10^{-2}
10^{-3}
10^{-4}
10^{-5}
$P_i(n)$
$P_{ext}(m)$
KCl
$E_p \simeq 1$ MeV
$P_i(n)$
$P_{ext}(m)$ (exp.)
$\delta = 0.3$
$P_{ext}(0) = 0.87$
$P_{ext}(m)$ (THEO.)
$\alpha = 0.25$
$\delta = 0.21$
$K = 2.12$
$P_{ext}(0) = 0.88$
$P_{ext}(m)$ (THEO.)
$\alpha = 0.45$
$\delta = 0.29$
$K = 1.74$
$P_{ext}(0) = 0.86$
0
5
10
15
20
25
30
35
n or m (NO OF ELECTRONS)
123688

Fig. 7c

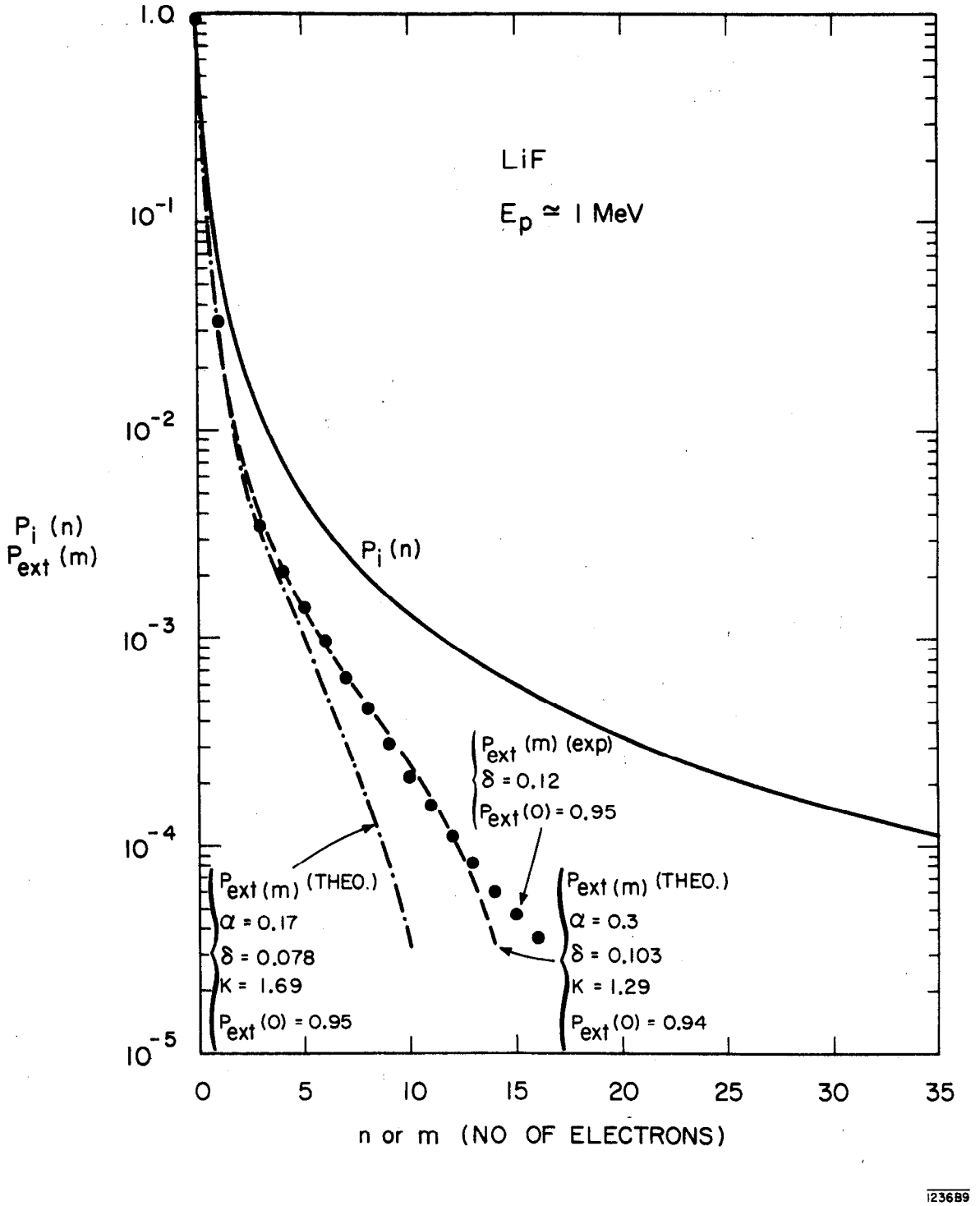
1.0
10^{-1}
10^{-2}
10^{-3}
10^{-4}
10^{-5}
P_i (n)
P_{ext} (m)
LiF
$E_p \simeq$ 1 MeV
P_i (n)
P_{ext} (m) (exp)
δ = 0.12
P_{ext} (0) = 0.95
P_{ext} (m) (THEO.)
α = 0.17
δ = 0.078
K = 1.69
P_{ext} (0) = 0.95
P_{ext} (m) (THEO.)
α = 0.3
δ = 0.103
K = 1.29
P_{ext} (0) = 0.94
0
5
10
15
20
25
30
35
n or m (NO OF ELECTRONS)
123689

Fig. 7d

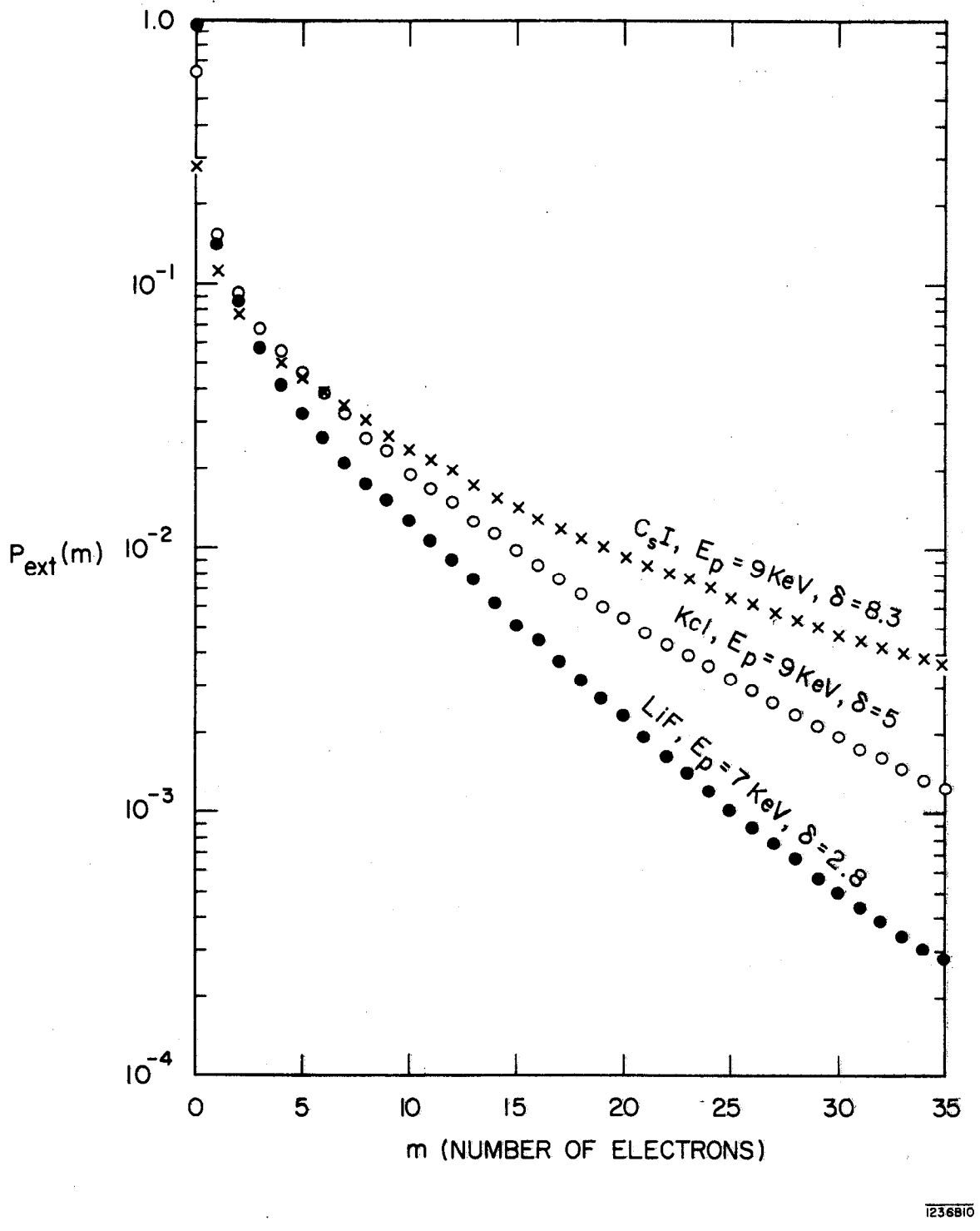
1.0
10^{-1}
10^{-2}
10^{-3}
10^{-4}
$P_{ext}(m)$
0
5
10
15
20
25
30
35
m (NUMBER OF ELECTRONS)
C_sI, $E_p = 9$KeV, $\delta = 8.3$
KCl, $E_p = 9$KeV, $\delta = 5$
LiF, $E_p = 7$KeV, $\delta = 2.8$
1236810

Fig. 8

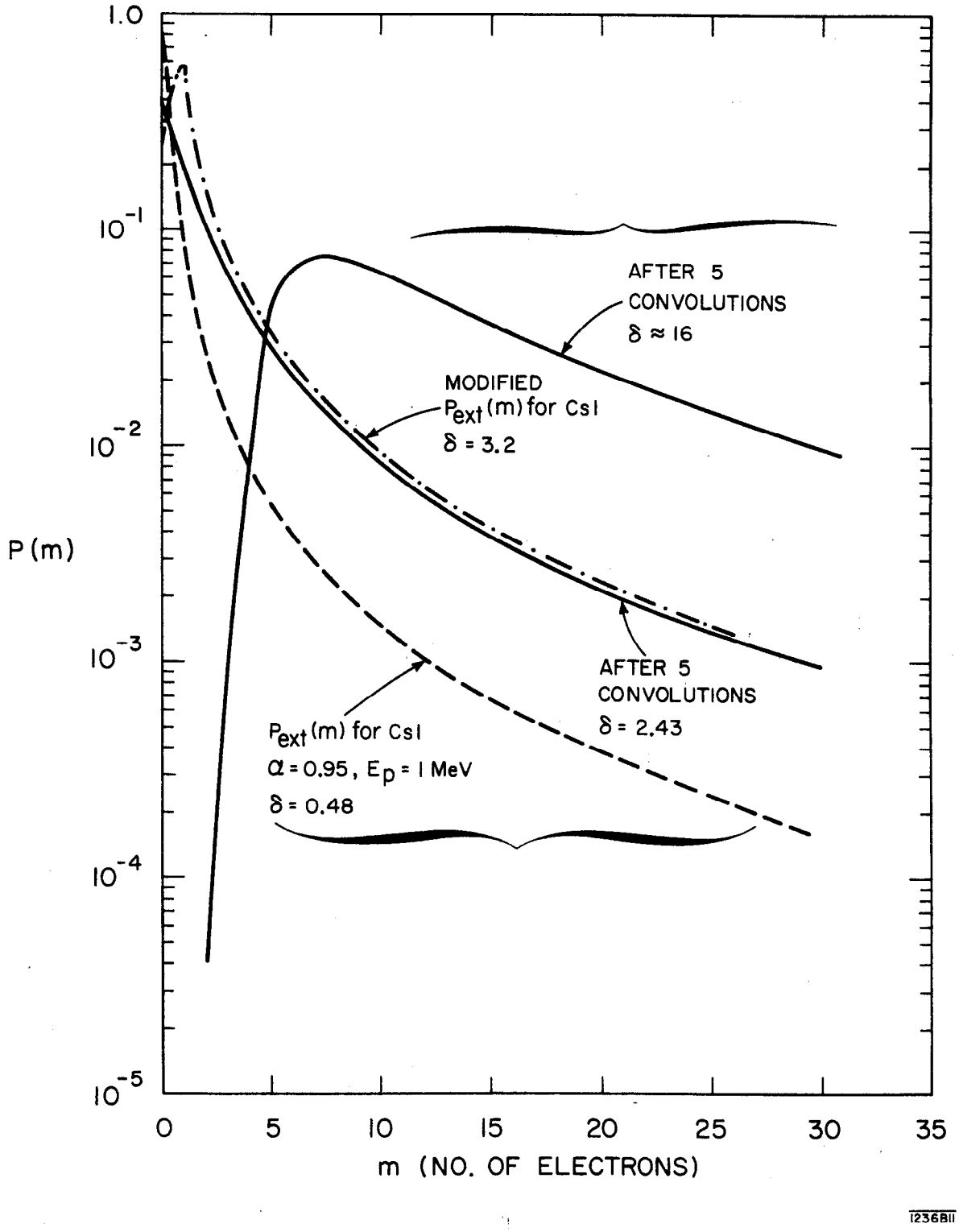
1.0
10^{-1}
10^{-2}
10^{-3}
10^{-4}
10^{-5}
P(m)
AFTER 5
CONVOLUTIONS
δ ≈ 16
MODIFIED
P_{ext}(m) for CsI
δ = 3.2
AFTER 5
CONVOLUTIONS
δ = 2.43
P_{ext}(m) for CsI
α = 0.95, E_p = 1 MeV
δ = 0.48
0
5
10
15
20
25
30
35
m (NO. OF ELECTRONS)
1236B11

Fig. 9